

# LEARNING EULER FACTORS OF ELLIPTIC CURVES

ANGELICA BABEL, FRANÇOIS CHARTON, EDGAR COSTA, XIAOYU HUANG, KYU-HWAN LEE,  
DAVID LOWRY-DUDA, ASHVNI NARAYANAN, AND ALEXEY POZDNYAKOV

**ABSTRACT.** We apply transformer models and feedforward neural networks to predict Frobenius traces  $a_p$  from elliptic curves given other traces  $a_q$ . We train further models to predict  $a_p \bmod 2$  from  $a_q \bmod 2$ , and cross-analysis such as  $a_p \bmod 2$  from  $a_q$ . Our experiments reveal that these models achieve high accuracy, even in the absence of explicit number-theoretic tools like functional equations of  $L$ -functions. We also present partial interpretability findings.

## 1. INTRODUCTION

When must different elliptic curves give different Euler factors (or Frobenius traces  $a_p$ )? By a result of Serre, see [Ser81, Théorème 5] and [BK16, Corollary 4.8], under the Riemann hypothesis for Artin  $L$ -functions, if  $E_1$  and  $E_2$  are two  $\overline{\mathbb{Q}}$ -nonisogenous elliptic curves over some number field and neither has complex multiplication, then there exists a prime  $p \nmid N$  of size  $O(\log^2(N))$  such that  $a_p(E_1) \neq a_p(E_2)$ , where  $N$  is the product of the absolute conductors of  $E_1$  and  $E_2$ . Thus a finite set of  $a_p(E)$  values determines all others. However, even when enough  $a_p(E)$  values are provided to uniquely identify the isogeny class, no efficient algorithm is known for determining the remaining  $a_p(E)$  values from this finite set, given a bound on the conductors.

Motivated by this challenge, we investigate the extent to which machine learning (ML) can predict Frobenius traces associated with elliptic curves. More precisely, given a finite subset  $a_p(E)$  values, we explore whether ML models can successfully infer other values and, in doing so, shed light on underlying structural properties of elliptic curves. The interplay between machine learning and number theory has rapidly expanded in recent years ([AHL<sup>+</sup>, HLO22b, HLO22a, HLO23, HLOP24, KV23, Poz24, BBF<sup>+</sup>24]), and we aim to contribute to this emerging field. In particular, we will apply transformer models developed by the second-named author [Cha], along with feed-forward neural networks.

Our experimental approach in Section 3 centers on training transformer models to predict  $a_p$  for a specific  $p$  from a selection of  $a_q$  values. Initial results show that models achieve surprisingly high accuracy when predicting  $a_{97}$  from  $a_q$  with  $q < 97$ , suggesting that some intrinsic patterns in the Frobenius traces are being captured. We also trained models to predict  $a_2$  and  $a_3$  for curves with good reduction at these primes. To better understand what ML models *learn*, we examine principal component analysis (PCA) plots for embeddings in the learning process. These plots reveal modular behavior, suggesting that the models might be learning congruences modulo 2 or 4. This observation naturally leads us to conduct experiments to learn  $a_p \pmod{2}$  from  $a_q$  values, where we again observe high accuracy.

Building on these observations, it is natural to try to predict  $a_p \pmod{2}$  from  $\{a_q \pmod{2}\}$ . We do this in Section 4. However, this approach introduces certain complications. Notably, reduction modulo 2 produces duplicates in the dataset, causing significant overlap between test and training

---

*Date:* February 17, 2025.

sets. Additionally, this reduction results in indeterminacy of  $a_p \pmod{2}$  for identical tuples  $\{a_q \pmod{2}\}$ . To address these issues, we adopt two strategies: first, we remove duplicates. Second, since the proportion of indeterminate cases is small for conductors up to  $10^7$ , we retain these cases and conduct experiments with caution.

We also conduct experiments with feedforward neural networks to predict  $a_p$  or  $(a_p \pmod{2})$  from either  $\{a_q : q \neq p, q < 100\}$ ,  $\{a_q \pmod{2} : q \neq p, q < 100\}$  or  $\{\frac{a_q}{\sqrt{q}} \pmod{2} : q \neq p, q < 100\}$ . Models have comparable or lower performance. Saliency analysis suggests that the most important features might depend on input encoding. We describe these experiments and analysis further in Section 5.

It is surprising that ML models often successfully predict  $a_p \pmod{\ell}$  from remaining  $a_q \pmod{\ell}$  values, as in this case we don't have typical tools like  $L$ -functions and functional equations to directly solve for missing coefficients. Instead, one needs to enumerate all possible mod  $\ell$  Galois representations to deduce the right answer.

Our work provides partial but compelling experimental evidence that ML can effectively learn relationships among Euler factors and Frobenius traces. We provide evidence that our transformer models' predictions of  $a_p$  rely on implicitly predicting  $a_p \pmod{2}$  values. However, given the opaque nature of neural networks and transformers, the precise mechanisms underlying these predictions remain an open mystery at the moment and calls for further analysis.

## ACKNOWLEDGMENTS

We thank the Harvard Center of Mathematical Sciences and Applications and to the organizers of the Mathematics and Machine Learning Program in fall of 2024 for creating such an exciting, welcoming environment. We would also like to thank Mike Douglas and Drew Sutherland for their support, guidance, and advice.

Costa was supported by Simons Foundation grant SFI-MPS-Infrastructure-00008651 and by Simons Foundation grant 550033. KHL was partially supported by a grant from the Simons Foundation (#712100). DLD was supported by the Simons Collaboration in Arithmetic Geometry, Number Theory, and Computation via the Simons Foundation grant 546235. Ashvni thanks the Hooper-Shaw foundation and the Sydney Mathematical Research Institute for supporting her.

This research includes calculations carried out on HPC resources supported in part by the National Science Foundation through major research instrumentation grant number 1625061 and by the US Army Research Laboratory under contract number W911NF-16-2-0189.

## 2. ML ARCHITECTURES AND PRELIMINARIES

**2.1. Elliptic curves.** An elliptic curve over  $\mathbb{Q}$  is a smooth, projective curve  $E$  of genus 1 with a distinguished point at infinity  $O \in E(\mathbb{Q})$ . It can be described by a Weierstrass equation:

$$E : y^2 = x^3 + Ax + B, \quad A, B \in \mathbb{Q}.$$

One can associate to  $E$  an  $L$ -function, given by the Euler product

$$L(E, s) = \prod_p L_p(E, s).$$

At all but finitely many primes  $p$ , where  $E$  has good reduction, the local factor is

$$L_p(E, s) = \frac{1}{1 - a_p(E)p^{-s} + p^{1-2s}}$$

with the trace of Frobenius at  $p$  equal to

$$a_p(E) = p + 1 - |E(\mathbb{F}_p)|,$$

and  $|E(\mathbb{F}_p)|$  is the number of solutions to the defining equation modulo  $p$ . At the remaining finitely many primes,  $E$  has bad reduction. The conductor  $N(E)$  is a product of powers of these primes with bad reduction, with exponents being dictated by whether  $E$  has multiplicative or additive reduction.

In the remaining sections, we perform experiments to predict the values  $a_p$ , which determine the Euler factors, given traces of Frobenius  $a_q$  for nearby primes  $q \neq p$ .

**2.2. Model Architecture: Transformers.** The transformer architecture, introduced in *Attention is All You Need* [VSP+17], has revolutionized deep learning by eliminating recurrence and instead leveraging self-attention mechanisms to process sequences in parallel. This design has proven highly effective in natural language processing (NLP) and is increasingly being applied across diverse domains. While we refer the reader to, for example, [ENO+21] for details on transformers, we briefly overview their architecture below.

A transformer consists of several key components:

- (1) **token embedding layer:** The first layer maps discrete tokens to continuous vector representations in a high-dimensional space. Given a vocabulary of size  $v$  and an embedding dimension  $d$ , each token is represented as a  $d$ -dimensional vector by multiplying its one-hot representation by a learnable  $v \times d$  matrix.
- (2) **positional encoding:** Since transformers lack recurrence, positional encodings are added to embeddings to introduce sequential information. These embeddings are learned, just like the token embedding.
- (3) **self-attention mechanism:** Self-attention enables each token to attend to all others in the sequence, allowing the model to capture long-range dependencies. The attention scores are computed using:

$$\text{Attention}(Q, K, V) = \text{softmax} \left( \frac{QK^T}{\sqrt{d_k}} \right) V$$

where  $Q$ ,  $K$ , and  $V$  represent queries, keys, and values derived from input embeddings and  $d_k$  is the dimension of the key vectors. Here, the softmax function ensures that attention scores form a probability distribution.

- (4) **multiple attention heads:** Transformers employ multiple attention heads, each focusing on different aspects of the input. These heads operate independently, and their contributions are summed before passing through subsequent layers. Given  $h$  attention heads, the multi-head attention mechanism is expressed as:

$$\text{MultiHead}(Q, K, V) = \sum_{i=1}^h \text{Attention}(QW_i^Q, KW_i^K, VW_i^V)W_i^O$$

where  $W_i^Q, W_i^K, W_i^V$ , and  $W_i^O$  are learned projection matrices for the  $i$ -th head. Attention heads can be interpreted as information-moving operations, transferring data between tokens. This movement is crucial for understanding how transformers capture relationships across sequences.

- (5) **feedforward network:** Each attention layer is followed by a position-wise feedforward network (FFN) containing one hidden layer of dimension  $4d$ , applied independently to each sequence position.
- (6) **residual connections and layer normalization:** Residual connections ensure stable gradient flow, while layer normalization improves convergence.

The transformer processes input sequences by first embedding the tokens and positions as two  $d$ -dimensional vectors, which are added together and fed into  $n$  transformer layers, composed of a multi-head attention and a feed-forward network. The output of the last layer is then decoded by a linear layer similar to the token encoder, which predicts, for each position in the output, the probabilities of the corresponding output token. The most likely output is the model prediction.

**2.3. Int2Int.** We utilize Int2Int [Cha], which implements a sequence-to-sequence transformer that is specialized to “translate” short sequences of integers into short sequences of integers. Our model is configured as an encoder-only architecture, as shown in Figure 1, with a total of 4,223,805 trainable parameters. We adopt the same encoding as the *PositionalInts* encoding in Int2Int for the inputs, where each integer is represented by a token indicating its sign followed by a token for its absolute value. For instance, the list of integers  $-1, 2, 5$  is converted to the string “- 1 + 2 + 5”. To handle output values, we apply a right shift so that all values are nonnegative. For instance, the smallest output value  $-2$  is mapped to the string “0” in the  $a_2$  prediction task.

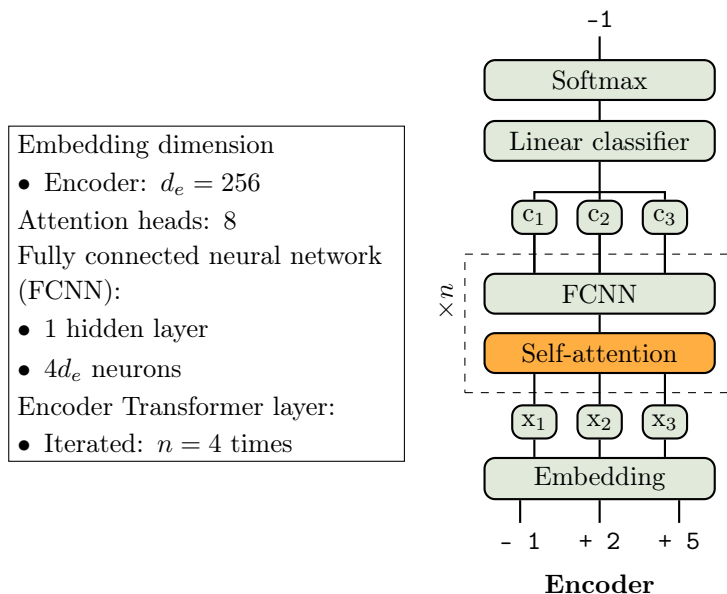


FIGURE 1. We implement an encoder only transformer architecture using Int2Int.

## 2.4. Performance metrics.

**2.4.1. Accuracy.** In the case of binary classification on balanced datasets, the most instructive performance metric is accuracy, which measures the proportion of correct predictions. We use this metric in the experiments in Sections 4 and 5.

2.4.2. *Matthews Correlation Coefficient.* Another performance metric is the the Mathews correlation coefficient (MCC), which is especially useful for unbalanced binary classification experiments. We use the MCC and a modified version as described below in all our experiments.

For binary classification experiments, the MCC is defined as in [Mat75] by

$$\text{MCC} := \frac{TP \times TN - FP \times FN}{\sqrt{(TP + FP)(TP + FN)(TN + FP)(TN + FN)}},$$

where  $TP, FP, TN$  and  $FN$  are the number of true positives, false positives, true negatives and false negatives, respectively. The MCC attains a value in the range  $[-1, 1]$ , where 1 indicates perfect prediction, 0 indicates no correlation between predictions and true values, and  $-1$  indicates perfectly wrong classification. For a balanced binary classification experiment, one obtains the accuracy ACC is obtained by  $\text{ACC} = \frac{\text{MCC} + 1}{2}$ .

One of the generalizations of MCC to multiclass experiments is given in [Gor04] by the formula

$$\text{MCC} := \frac{\sum_k \sum_l \sum_m C_{kk} C_{lm} - C_{kl} C_{mk}}{\sqrt{\sum_k (\sum_l C_{kl}) (\sum_{k' | k' \neq k} \sum_{l'} C_{k'l'})} \sqrt{\sum_k (\sum_l C_{lk}) (\sum_{k' | k' \neq k} \sum_{l'} C_{l'k'})}},$$

where  $C_{ij}$  is the  $(i, j)$  entry in the confusion matrix  $C$ . This generalization is implemented in sklearn, and is the one we use in our multiclass experiments.

2.5. **Datasets.** We concentrated our efforts on isogeny classes of elliptic curves with small conductors, specifically those less than  $10^7$ . In particular, we started with a dataset created by Andrew Sutherland that extends the one in [SW02], constructed using similar methods and including elliptic curves with conductors up to  $10^8$ . From this superset, we extracted two subsets, ECQ6 and ECQ7 [Sut], of sizes 3,607,212 and 28,257,805, respectively, corresponding to the isogeny classes with conductors less than  $10^6$  and  $10^7$ .

Some experiments in Section 5 are performed on isogeny classes of curves with conductor between  $2^{15}$  and  $2^{16}$  in the LMFDB [LMF24]. These curves form a subset of ECQ6.

### 3. LEARNING $a_p$ FOR SMALL PRIMES

In this section, we examine if one can learn the true value  $a_p$  given nearby traces of Frobenius. We restrict ourselves to an input sequence  $(a_q)_{q \neq p, q \leq 100}$  of 24 primes and curves of conductor less than  $10^6$ .

The sequential nature of the data  $(a_q)_{q \neq p, q \leq 100}$  is well-suited for sequence-to-sequence models such as recurrent neural networks (RNNs) or transformers. With some limitations, transformers have been taught number theory tasks such as modular arithmetic [SAWL24] and predicting the greatest common divisor [Cha23]. As seen in [Cha23], the ability of transformers to learn problem-specific embeddings could be particularly useful for number theory applications.

3.1. **Methodology.** For the following three experiments, we employed a transformer model as implemented in Int2Int [Cha] with an encoder-only architecture. The vocabulary consists of integers  $0 \leq n \leq 19$ , signs  $+, -$ , as well as special tokens. The model architecture follows the description in Section 2.3. We used the Adam optimizer and a learning rate of  $3 \cdot 10^{-5}$ . Each task is treated as a classification task, with 39 classes for predicting  $a_{97}$ , 5 classes for  $a_2$ , and 7 classes for  $a_3$ .

The training examples consist of sequences  $(a_q)_{q \neq p, q < 100}$  of length 24, for which we predict  $a_p$ . This data represents isogeny classes of curves with good reduction at  $p$  from the dataset ECQ6. In

each case, we reserved a test set of 10k isogeny classes sampled uniformly at random, distinct from the training set.

**3.2. Results.** We describe in detail the results of the experiment for learning  $-19 \leq a_{97} \leq 19$ . After 100 epochs of 3.5 million training examples, the transformer model reached a maximum accuracy of 0.4923 and maximum MCC of 0.4711. In Figure 2, we show the proportion of cases where the model predicts a given value as a function of its true value. The main diagonal corresponds to perfect predictions.

Although the experiment for predicting  $a_{97}$  performed well compared to the baseline precision of 0.082, which is the proportion of the most common class, it cannot serve as a prototype for generating sequential values  $a_{97}, a_{101}, a_{103}, \dots$ . One of the potential causes of low performance could be the large number of classes to be predicted. Therefore, we trained two additional models to predict  $a_p$  which contains fewer classes, in particular  $a_2$  and  $a_3$ .

The results for predicting  $-2 \leq a_2 \leq 2$ ,  $-3 \leq a_3 \leq 3$  and  $-19 \leq a_{97} \leq 19$  are summarized in Table 1. In addition, Figure 3 shows the heat maps of the normalized confusion matrices for predicting  $a_2$  and  $a_3$ . The alternating color intensity along the rows indicates that the predicted values frequently match the true values modulo 2. We also explore this modular phenomenon further in Section 4, where we predict  $a_p \pmod{2}$ . Moreover, we visualize the 2D PCA projections of their learned embeddings in Section 6 to understand the underlying modular structure of these embeddings.

We note that in both Figures 2 and 3, the models often correctly predict  $a_p$  up to sign. In Table 1, we also record the sign-agnostic MCC of  $|\text{predicted } a_p| \stackrel{?}{=} |\text{true value of } a_p|$ .

In all three cases, the models struggle to distinguish the sign of  $a_p$ . In Section 5.2, we perform a binary classification neural network-based experiment to predict the value  $a_2 = \pm 1$ .

$p$	$N_{\text{samples}}$	$N_{\text{epochs}}$	Epoch size	$N_{\text{classes}}$	Max Test MCC	Max Sign-Agnostic MCC
2	722,204	200	700,000	5	0.5822	0.7345
3	1,210,417	200	1,200,000	7	0.5205	0.6908
97	3,550,727	100	3,500,000	39	0.4711	0.6266

TABLE 1. Predicting  $a_p$  for  $p \in \{2, 3, 97\}$  with an encoder-only transformer. We record both the maximum MCC as well as the maximum sign-agnostic MCC.

#### 4. LEARNING $a_p \pmod{2}$

The confusion matrix results in Figure 2 and Figure 3 indicate that the models' inference of  $a_p$  rely, at least in part, on implicitly inferring  $a_p \pmod{2}$ . In particular, the models should be capable of explicitly determining  $a_p \pmod{2}$ . To validate this hypothesis, we conducted two sets of experiments focused on learning  $a_p \pmod{2}$  for all  $p < 100$ .

**4.1. Given  $\{a_q\}_{q \neq p, q < 100}$  for curves with good reduction at  $p$ .** In each case of  $p$ , the training set includes 2 million curves with good reduction at  $p$ , except for  $p = 2, 3, 5$ , sourced from ECQ6. The test set consists of 10,000 distinct curves not present in the training set. For  $p = 2, 3, 5$ , the training set sizes are 632,205, 1,120,417, and 1,906,257, respectively, due to the good reduction condition. The dataset is intentionally unbalanced for this experiment for two reasons. First, to reflect real-world deployment scenarios where class distributions are naturally imbalanced. Second,

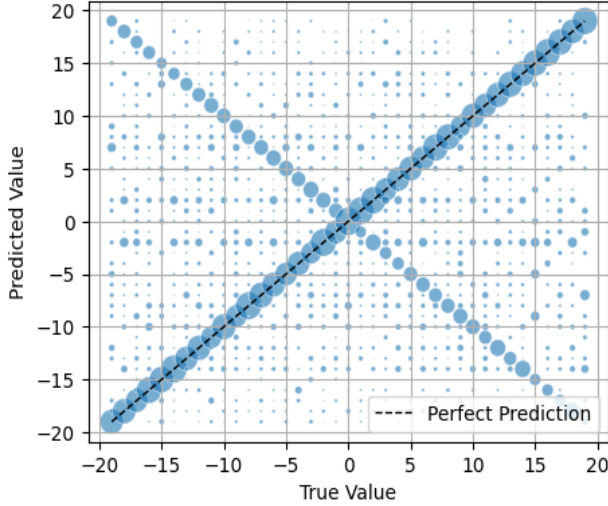


FIGURE 2. Predicting  $a_{97}$ . Proportion of cases where the model predicts a given value as a function of its true value.

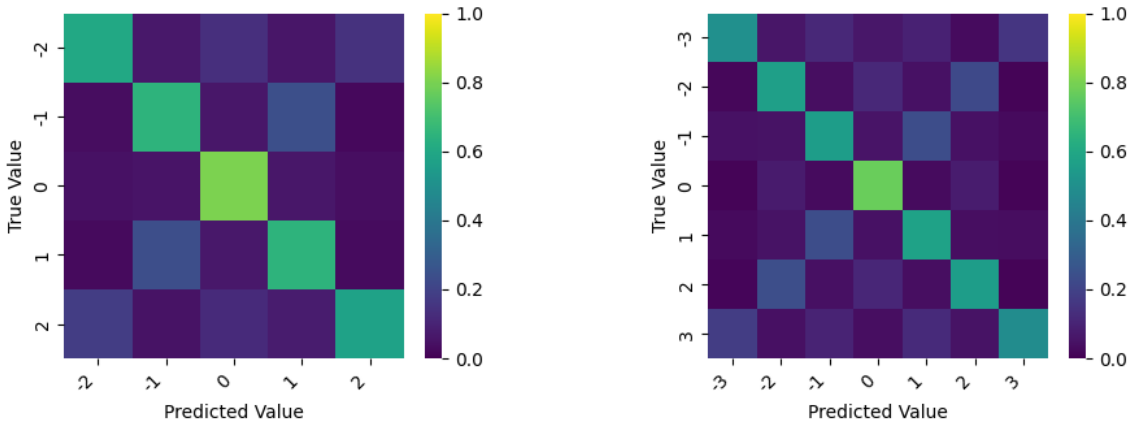


FIGURE 3. Confusion matrix heat map for predicting  $a_2$  (left) and  $a_3$  (right).

the majority class ratio (where  $a_p \equiv 0 \pmod 2$ ) ranges from 52.45% for  $p = 2$  to 72.62% for  $p = 97$  in the combined training and test datasets, as shown in Figure 4, which is within acceptable limits.

The transformer model was implemented in Int2Int as described in Section 2.3. We used the Adam optimizer and a learning rate of  $5 \cdot 10^{-5}$  for the results here. The accuracy and MCC results are presented in Figure 5.

Interestingly, the 2D PCA projections of the learned embeddings closely resemble those from Section 3, both presented in Section 6, where the models predict the true  $a_p$ . As discussed in Section 6, this similarity suggests that the models in Section 3 may be inferring  $a_p$  values based on their mod 2 representations.

**4.2. Given  $(a_q \pmod 2)_{q \neq p, q < 100}$  for curves of good reduction at  $p$  and removing duplicates.** Comparing the previous experiment with one on the same dataset, but whose input is the sequence modulo 2,  $(a_p \pmod 2)_{p \neq q, p < 100}$ , poses two problems.

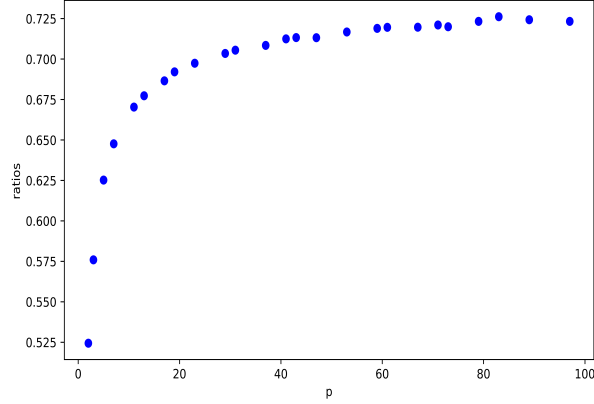


FIGURE 4. The ratios of curves with  $a_p \equiv 0 \pmod{2}$  for various  $p < 100$  when curves have good reduction at  $p$ . There is a consistent bias of  $a_p \equiv 0 \pmod{2}$  when  $p$  is not “small”.

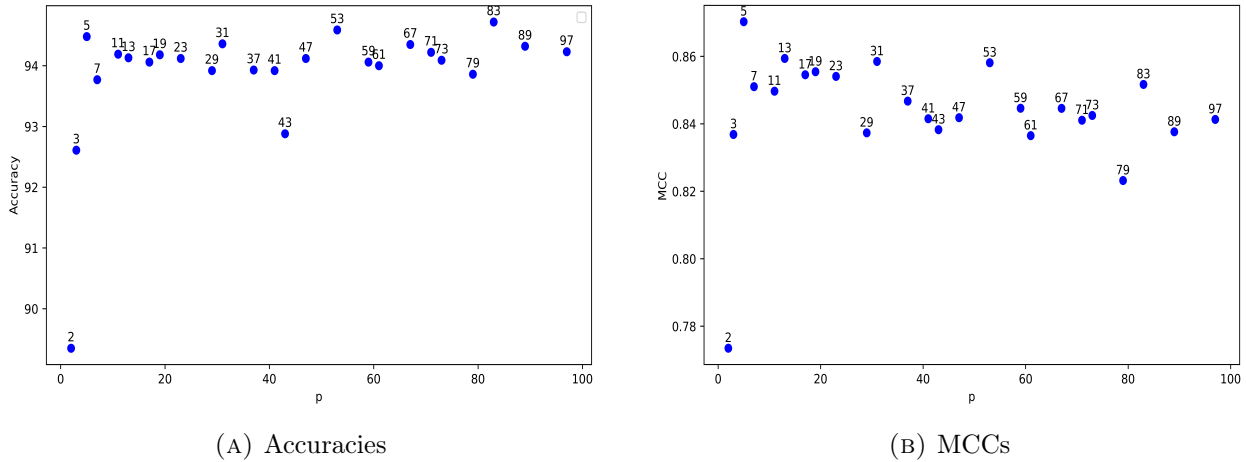


FIGURE 5. The results of predicting  $a_p \pmod{2}$  using  $\{a_q\}_{q \neq p, q < 100}$  for curves with good reduction at  $p$  show that, except for  $p = 2, 3, 43$ , the model achieves accuracies close to 0.94. The highest accuracy, 0.9472, occurs at  $p = 83$ , while the lowest, 0.8935, is observed at  $p = 2$ . Similarly, the model achieves MCC around 0.84, except for  $p = 2, 79$ . The highest MCC, 5, 0.8703, is recorded at  $p = 5$ , whereas the lowest, 0.7735, occurs at  $p = 2$ .

The first problem is of significant overlap between training and test data. Despite the fact that theoretically there are  $\sim 33.5$  million binary tuples of length 25, **ECQ6** only contains  $\sim 0.7$  million representatives modulo 2. Once we reduce the dataset modulo 2, more than 80% of the test data is seen in the training data. The second issue is one of indeterminacy, as the same input sequence  $(a_q \pmod{2})_{q \neq p, q < 100}$  can yield different output  $a_p \pmod{2}$ .

We create a new dataset that addresses the first issue by removing duplicates, i.e. we select a single representative for a given tuple  $(a_q \pmod{2})_{q < 100}$  containing both input and output. However, this significantly reduces the dataset size when restricted to isogeny classes in **ECQ6**. Therefore, for this series of experiments only, we use curves from **ECQ7** instead. In particular, we include 5 million

isogeny classes of curves, containing all representatives mod 2 in ECQ6 as well as approximately 4.3 million representatives in ECQ7 with the lowest conductor.

In the following experiments, we train models to predict  $a_p \pmod{2}$  for each prime  $p < 100$  on the dataset described above. For each prime, we first remove curves with bad reduction at  $p$ , then balance the dataset according to  $a_p \pmod{2}$ . After balancing, the training set at each prime has between 5 – 11.5 % indeterminates; when restricting to curves of conductor up to  $10^6$ , the proportion of indeterminates is reduced to 1 – 2.5 %.

We reserve 15,000 examples for a test set, distinct from the training set, where 5,000 curves in each of the following conductor ranges:  $10^4 \leq N(E) < 10^5$ ,  $10^5 \leq N(E) < 10^6$  and  $10^6 \leq N(E) < 10^7$ . We use an encoder-only transformer as described in Section 2.3. We ran each experiment for 1,000 epochs of size 100,000 training examples.

Figure 6 shows the maximum attained MCC across the three conductor ranges for each prime. As expected, the performance is reduced for curves of the highest conductor range  $10^6 \leq N(E) < 10^7$ .

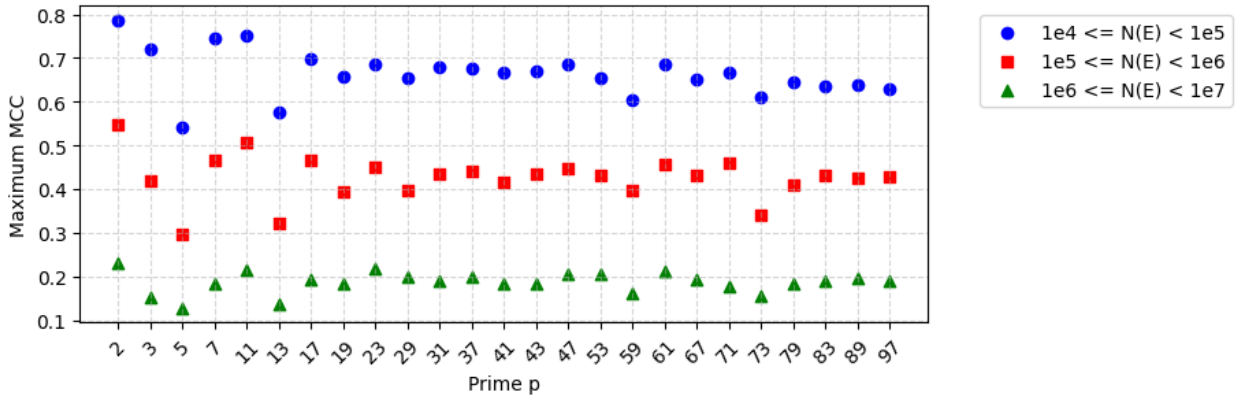


FIGURE 6. Maximum MCC achieved in three conductor ranges for  $a_p \pmod{2}$  for various primes  $p < 100$ .

## 5. NEURAL NETWORK EXPERIMENTS

To explore the significance of the transformer architecture used above, we provide several experiments that use a standard feedforward neural network (FFN) to predict  $a_p$ . For one set of experiments, we use an FFN to predict  $a_p \pmod{\ell_p}$  for  $p \in \{2, 97\}$  and  $\ell_p \in \{0, 2\}$ <sup>1</sup>. As features we use  $\{a_q \pmod{\ell_q} : q < 10^2, q \neq p\}$  where  $\ell_q \in \{0, 2\}$ . The models were trained and tested on all of the curves in ECQ6 with good reduction at  $p$  and with duplicates removed. All neural networks have layers of width  $[2^{n+m}, 2^{n+m-1}, \dots, 2^{n+1}, 2^n]$  for some  $m, n$ . All of the features and labels were represented by a one-hot encoding. We always use  $N_{\text{samples}} - 10^4$  curves for training and  $10^4$  curves for testing. We always use AdamW optimizer with learning rate  $10^{-4}$  and weight decay 0.1, and we train for  $10^4$  epochs.

One might expect that small primes carry more information about the  $L$ -function than larger primes. However, we obtain conflicting results, which require further investigation. We explore some observations on which  $a_q$  appear to be most important for predicting  $a_p$  by examining saliency plots.

<sup>1</sup>We use the convention  $a \equiv b \pmod{0} \iff a = b$ .

$p$	$\ell_p$	$\ell_q$	$N_{\text{params}}$	$N_{\text{samples}}$	Test Acc	Test MCC
2	0	0	136,581	732,205	0.4136	0.2412
2	2	0	136,482	732,205	0.7364	0.4770
2	2	2	16,674	292,107	0.6651	0.3300
97	0	0	1,709,353	2,000,000	0.2602	0.2268
97	2	0	136,482	2,000,000	0.8691	0.6524
97	2	2	55,842	697,051	0.7433	0.4228

TABLE 2. Neural network experiments

Figure 7 shows saliency plots for the experiments in Table 2 in the same order as presented in the table.

We compare the saliency plot for the experiment for predicting  $a_{97} \pmod{2}$  from subfigure (E) to five transformer-based experiments with architecture as described in Section 2.3. In each experiment, we exclude different sets of 3 primes. The models have the same encoder-only architecture and hyperparameters as the models in Section 3, except that we train the models for 150 epochs of size 100,000 curves. We balance the datasets and use 1,960,662 curves, half of which have  $a_{97} \equiv 0, 1 \pmod{2}$ .

This comparison is appropriate since both the previous neural network experiment and the transformer initially treat the  $a_q$  values as one-hot encodings. We record the maximum MCC in Table 3. We note that the experiments which exclude larger primes usually have lower performance.

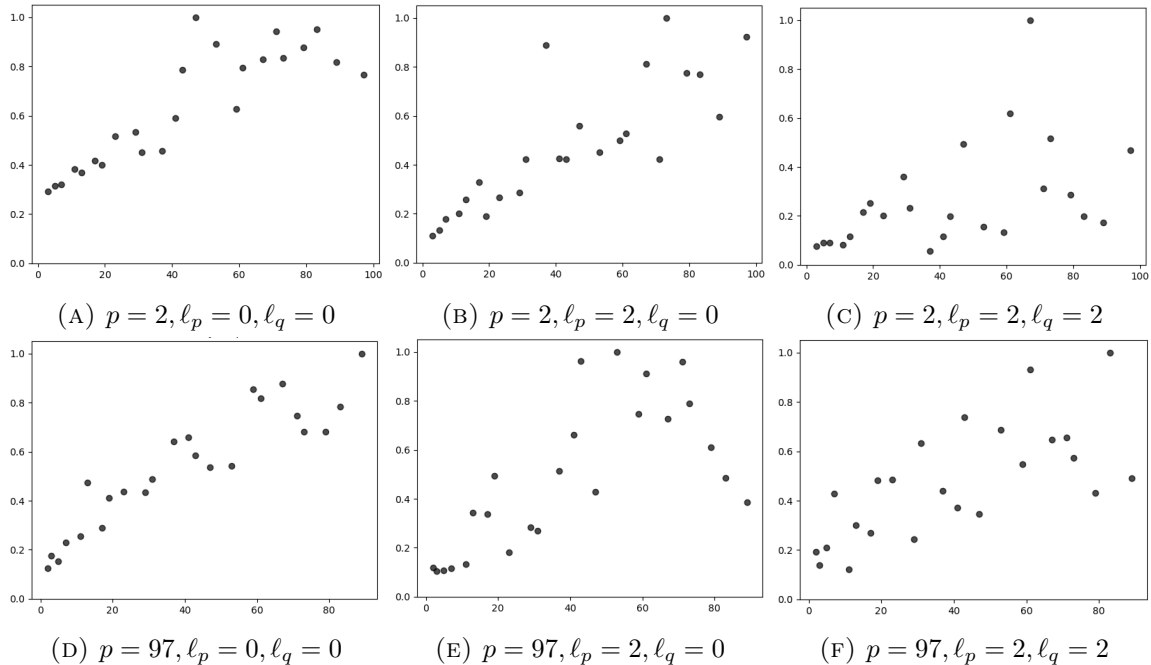


FIGURE 7. Saliency plots (prime  $q$  against saliency of  $a_q \pmod{\ell_q}$ ) for neural network experiments in Table 2

Primes excluded	Maximum Test MCC
2, 3, 5	0.8262
13, 17, 19	0.7870
31, 37, 41	0.7848
43, 53, 71	0.7850
79, 83, 89	0.7658

TABLE 3. Maximum MCC values for predicting  $a_{97}$  from  $(a_q)_{q < 97}$  and excluding  $a_q$  values for triples of primes. Compare with the saliency map in Subfigure (E) in Figure 7.

5.1. **A different normalization.** We performed some experiments to predict  $a_p \pmod{2}$  using  $\frac{a_q}{\sqrt{q}} < 2$  as input. This is in the same style as the experiments conducted in 5.2.

We use the dataset ECQ6, where we conducted experiments in the same style for a balanced dataset (size 1,000,000) with conductors between  $10^5$  and  $10^6$ . For  $p = 97$ , we obtained an accuracy of about 0.86, with an MCC of 0.7486, which is comparable to the performance of the FNNs in the previous section. The saliency plots (8), in this case, however, do not show an independence from smaller primes. In fact, the small and middle primes seem to be the most important features. This is different to what we noticed with results from experiments using one-hot encoding, leading us to believe that a difference in style of encoding could lead to a difference in the importance of primes. Moreover, as expected, the conductor seems to be playing the most important role, while the root number has importance comparable to other prime features.

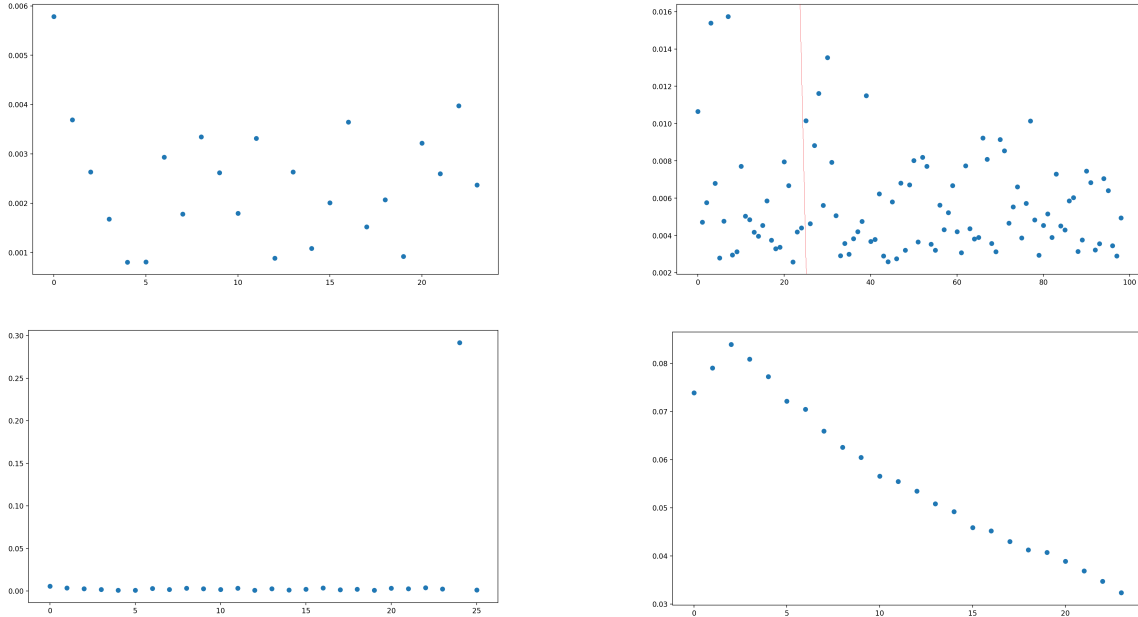


FIGURE 8. Saliency plots for important features. The top left is for the 24 primes governing  $a_{97} \pmod{2}$ , the top right shows the importance of primes when using the first 100 primes. The bottom left shows the same plot with conductor and root number added as well, while the bottom right shows a saliency plot for  $|a_2| = 1$ .

5.2. **Neural net experiments for  $a_2 \in \{\pm 1\}$ .** Initial models are trained on curves between conductors  $2^{15}$  and  $2^{16}$  (between  $10^5$  and  $10^6$ ) present in the LMFDB. For each curve in the dataset,  $\frac{a_q}{\sqrt{q}} < 2$  values are given for the first 100 primes, except  $a_2$ , which is not normalized. The conductor and root number are also passed separately.

The total size of the balanced dataset is 71,643. Given the small size, we use 10% of this as the test set. The training set is further scaled, while a test set is scaled using the same values. A one hot encoding is used to capture the output, and a final softmax layer ensures that the probabilities of the logits is returned.

A relatively small neural net with 2 hidden layers of dimensions 64 and 32 respectively gives the best result, with the AdamW optimizer having a dropout of 0.05, weight decay of 0.01 and learning rate  $10^{-4}$ . After 15,000 epochs, we have an accuracy of 0.9137 on the test set.

We then repeated a similar experiment on the larger dataset ECQ6, which contains 1,674,207 datapoints with  $a_2 \in \{\pm 1\}$ . Using the same parameters and replacing the final softmax layer with a sigmoid layer, after 250 epochs and with a batch size of 1,024, we obtain an accuracy of 0.6384 with an MCC of 0.3049. The striking thing about this model is its saliency graph, where the importance of the features seems to be linearly decreasing in nature, as shown in Figure 8.

## 6. VISUALIZING MOD $\ell$ STRUCTURE IN LEARNED EMBEDDINGS AND REPRESENTATIONS

This section first examines the 2D PCA projections of the learned initial embeddings from the experiments conducted in Section 3 and Section 4. Our goal is to investigate whether the models in Section 3 predict  $a_p$  values by first learning to predict  $a_p \pmod{2}$  as an intermediate step. Although tools for interpreting neural network-based models, including transformers, remain limited (for examples exploring how transformers learn some algorithmic tasks, see [NCL<sup>+</sup>23, LKN<sup>+</sup>22, ZLTA24, QB23, CCN23, HLV24, Cha23]), the embeddings reveal clear patterns suggesting that the models encode distinctions based on their mod- $\ell$  residues, with a particular emphasis on parity. The visualizations presented in this section were generated using [Bab].

We further analyze the experimental results across several tasks: (1) predicting the exact values of  $a_p$  and (2) predicting their residues modulo  $\ell$  for  $\ell \in \{2, 4\}$ . The model demonstrates significantly better performance in the  $a_p \pmod{2}$  and  $a_p \pmod{4}$  tasks. Together with the PCA projections of the initial embeddings and the confusion matrix in Figure 2, which reveals the model’s difficulty in distinguishing values sharing the same parity, these results strongly suggest that the transformer model relies on predicting  $a_p \pmod{2}$  as an intermediate step in learning to predict the full  $a_p$  values.

Lastly, we implemented an additional encoder-decoder transformer model to predict  $a_2$ . The PCA projections of the decoder’s hidden states and encoder’s initial embeddings indicate that the model relies on inferences of  $a_p \pmod{\ell}$  for multiple  $\ell$ .

**6.1. 2D PCA Projections of Initial Embeddings.** The vocabularies used in the experiments described in Section 3 and Section 4 consist of tokens including integers  $0 \leq n \leq 19$ , the symbols + and −, and special tokens like <eos>, which indicates the end of a sentence. Following [ENO<sup>+</sup>21], the initial step of learning involves the transformer model learning a context-free token embedding  $W_E$ , which maps each token to a meaningful vector representation in  $\mathbb{R}^{256}$ .

6.1.1. *Predicting  $a_p$ .* In Figure 9, we plot the 2D PCA projection of the initial embeddings for +, − and integer values  $0 \leq n \leq 19$  for the  $a_p$  prediction task.

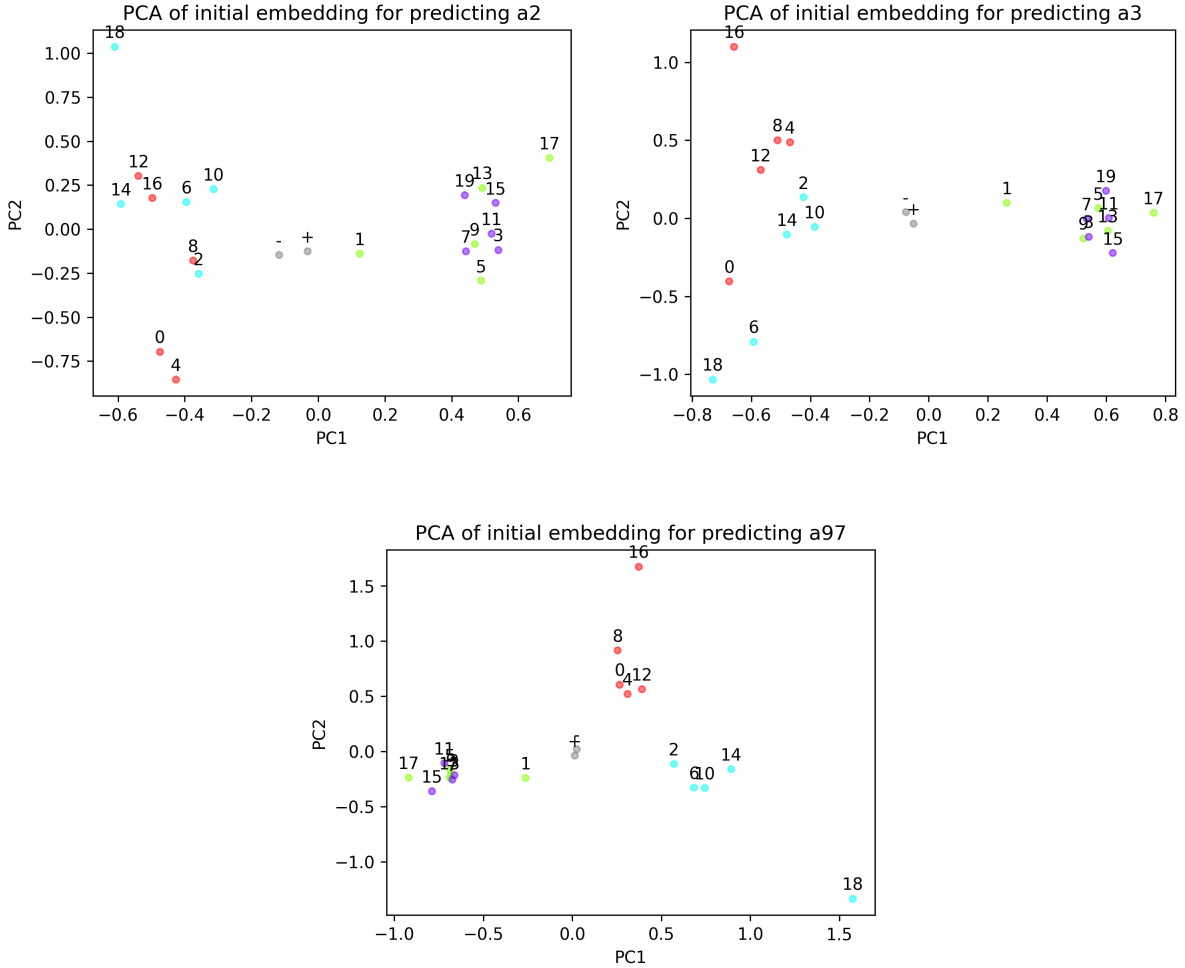


FIGURE 9. PCA plots of the initial embeddings for predicting  $a_2$ ,  $a_3$ , and  $a_{97}$  are shown:  $a_2$  (upper left),  $a_3$  (upper right), and  $a_{97}$  (bottom). Red, green, blue, and purple dots represent  $a_q \equiv 0, 1, 2, 3 \pmod{4}$ , respectively. All show clear separation between odd and even integers. For  $p \in \{3, 97\}$ , we observe further differentiation between  $a_q \equiv 0 \pmod{4}$  and  $a_q \equiv 2 \pmod{4}$ .

In Figure 9, there is a clear clustering based on the parity of the tokens in all cases, with further differentiation between  $a_q \equiv 0 \pmod{4}$  and  $a_q \equiv 2 \pmod{4}$  when predicting  $a_3$  and  $a_{97}$ . These plots suggest that all the models implicitly learn to distinguish  $a_q \pmod{2}$ , and might therefore learn to predict  $a_p \pmod{2}$  as an intermediate step.

In addition, in all cases, the  $+$  and  $-$  values cluster closely together near zero. As noted in Section 3, this may suggest that the models have difficulty distinguishing between positive and negative  $a_p$  values and establishing a meaningful representation for them.

6.1.2. *Predicting  $a_p \pmod{2}$ .* In Figure 10, we plot the 2D PCA projection of the initial embeddings for the  $a_p$  prediction task. The differentiation between modular-4 classes is similar to Figure 9 but slightly more pronounced.

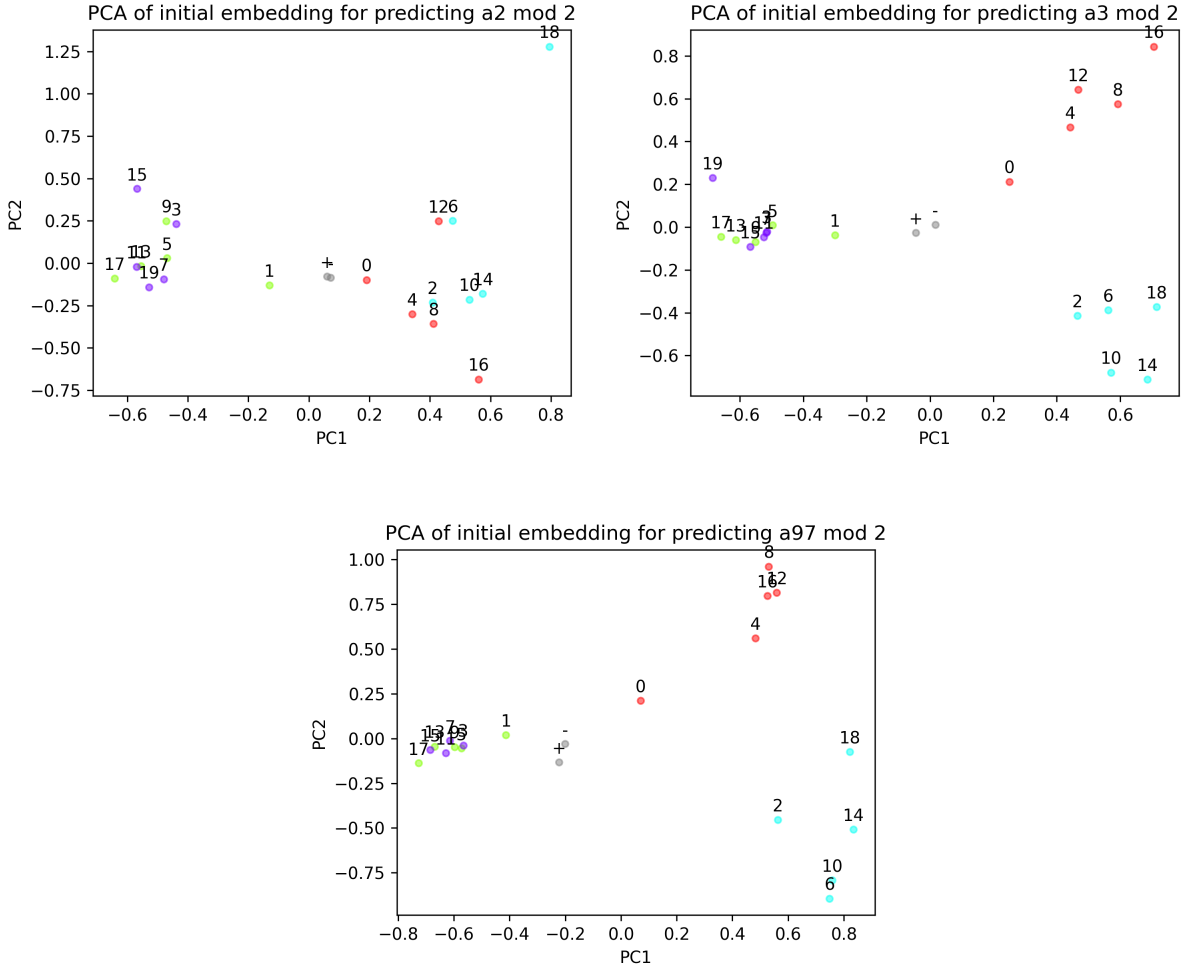


FIGURE 10. PCA plots of the initial embeddings for predicting  $a_2 \pmod 2$  (upper left),  $a_3 \pmod 2$  (upper right), and  $a_{97} \pmod 2$  (bottom). The distinction between modular-4 classes resembles that in Figure 9.

**6.2. Experiment Results Comparison.** To further demonstrate that the transformer’s learning relies on implicit predicting  $a_p \pmod 2$ , Table 4 reports the MCCs for  $a_p \pmod \ell$  derived from the true  $a_p$  predictions in Section 3, for  $p \in \{2, 3, 97\}$  and  $\ell \in \{2, 3, 4\}$ . These MCCs are computed by converting the labels to their modulo  $\ell$  values using the model trained on true  $a_p$  predictions. Notably, the performance for  $a_p \pmod 2$  and  $a_p \pmod 4$  predictions significantly surpasses that of predicting  $a_p$  and  $a_p \pmod 3$ , aligning with the model’s recognition of mod-2 and mod-4 classes observed in Figure 9. Moreover, the *Test MCC mod 2* results are consistent with, though slightly worse than, those in Section 4, where the model is specifically trained to predict  $a_p \pmod 2$ .

**6.3. An Encoder-Decoder Model.** For the purpose of visualizing decoder-specific learned embeddings and representations, we also trained an encoder-decoder transformer to predict  $a_2$ . The architecture and hyperparameters remain nearly identical to the previous models, with the only difference being the addition of a decoder containing one transformer layer. The architecture is depicted in Figure 11. Table 5 reports the performance of this experiment.

$p$	$N_{\text{samples}}$	$N_{\text{classes}}$	Test MCC	Test MCC mod 2	Test MCC mod 3	Test MCC mod 4
2	722,204	5	0.5822	0.7678	0.5385	0.6154
3	1,210,417	7	0.5205	0.7802	0.4893	0.5905
97	3,550,727	39	0.4711	0.7981	0.4702	0.6497

TABLE 4. Predicting  $a_p$  with an encoder-only model. The implied MCC results in Section 3 are obtained by converting the labels to their modulo  $\ell$  values and computing the MCC.

$p$	$N_{\text{samples}}$	$N_{\text{classes}}$	Test MCC	Test MCC mod 2	Test MCC mod 3	Test MCC mod 4
2	722,204	5	0.6178	0.7788	0.5807	0.6485

TABLE 5. Predicting  $a_2$  with an encoder-decoder model. The modular MCC results are obtained by converting the labels to their modulo  $\ell$  values and computing the MCC.

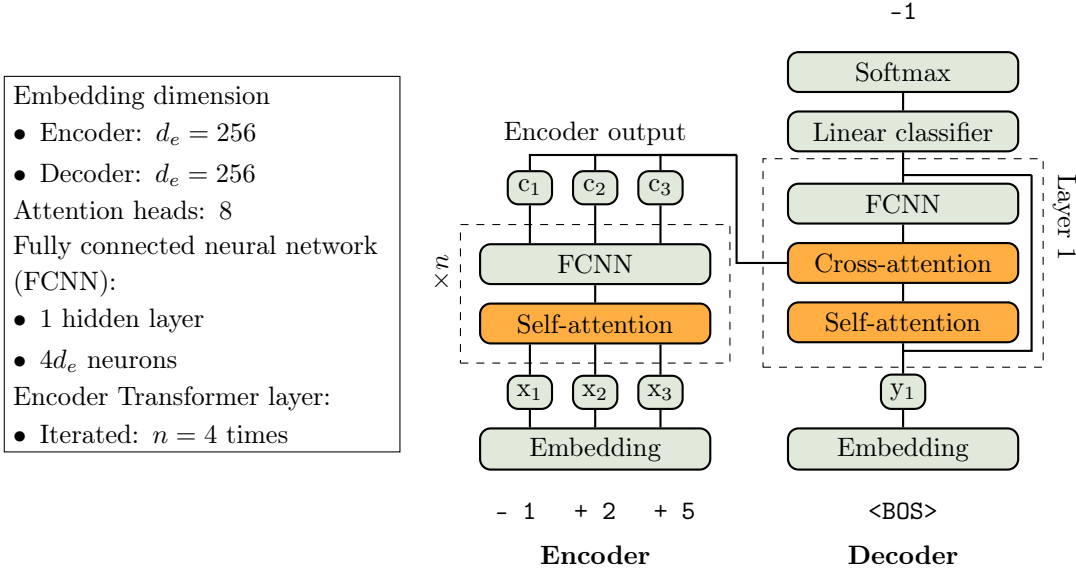


FIGURE 11. We also implement an encoder-decoder Transformer for further insights into  $a_2$  predictions using Int2Int.

As a result, we obtain a clear structure of the hidden states in the decoder compared to the encoder. Figure 12 shows the 2D PCA plot of the decoder’s hidden states after passing the model curves of low conductor up to  $10^4$ . The model distinguishes these elliptic curves by their  $a_2$  (mod 2) and  $a_2$  (mod 4) values after processing the  $a_q$  inputs. Additionally, the second principal component reflects a distinction between positive and negative values, possibly due to the model’s recognition of  $a_2$  (mod 3) values.

We also note differences in the learned initial embedding in the encoder, as shown in Figure 13. Compared to the encoder-only model used in Section 3 visualized in Figure 9, the encoder’s initial embeddings in this experiment contain clusters based both on parity and divisibility by 3,

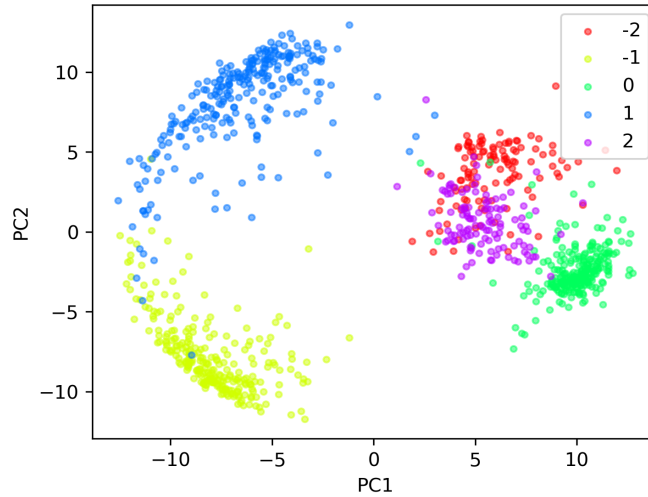


FIGURE 12. The 2D PCA of the model’s hidden states at the decoder transformer layer for predicting  $a_2$  with conductor up to  $10^4$ . The dots, representing the hidden states of curves, are separated by their residue classes mod-2 and mod-4 from left to right.

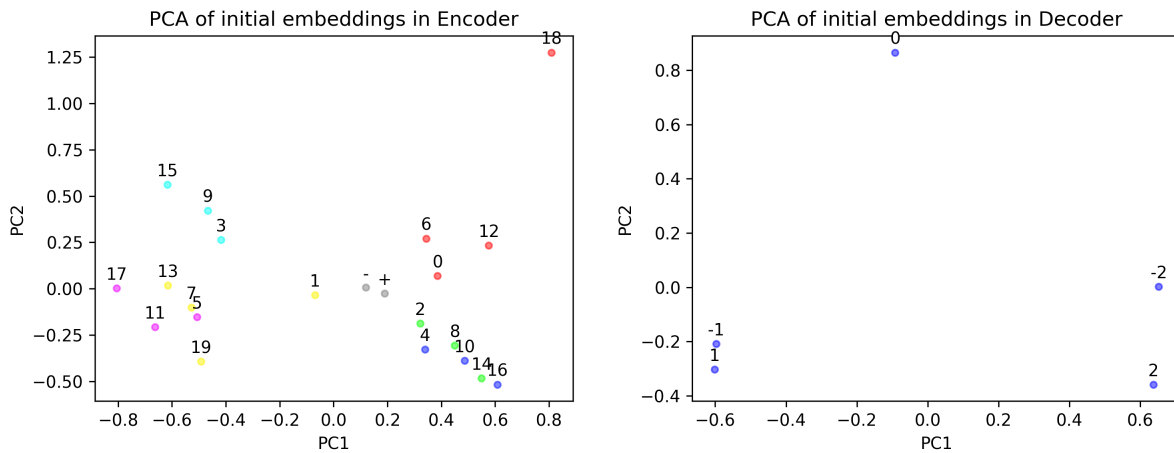


FIGURE 13. PCA plots of the initial embeddings in the encoder (left) and decoder (right) for predicting  $a_2$  with an encoder-decoder model. The encoder PCA shows a clear separation between even and odd integers, as well as integers divisible by 3. As a result, we observe clustering based on modulo 6.

resulting in clustering based modulo 6. Despite this clustering, the prediction of  $a_2 \pmod{3}$  does not outperform the prediction of  $a_2$ .

#### REFERENCES

- [AHL<sup>+</sup>] M. Amir, Y.-H. He, K.-H. Lee, T. Oliver, and E. Sultanow. On the machine-learning of the class number of real quadratic fields. In preparation.
- [Bab] Angelica Babei. Pca plotting for int2int. <https://github.com/ababei/Int2Int>.

- [BBF<sup>+</sup>24] Angelica Babei, Barinder S Banwait, AJ Fong, Xiaoyu Huang, and Deependra Singh. Machine learning approaches to the shafarevich-tate group of elliptic curves. *arXiv preprint arXiv:2412.18576*, 2024.
- [BK16] Alina Bucur and Kiran S Kedlaya. An application of the effective sato-tate conjecture. *Frobenius distributions: Lang-Trotter and Sato-Tate conjectures*, 663:45–56, 2016.
- [CCN23] Bilal Chughtai, Lawrence Chan, and Neel Nanda. A toy model of universality: Reverse engineering how networks learn group operations. In *International Conference on Machine Learning*, pages 6243–6267. PMLR, 2023.
- [Cha] François Charton. Int2int. <https://github.com/f-charton/Int2Int>.
- [Cha23] François Charton. Can transformers learn the greatest common divisor? *arXiv preprint arXiv:2308.15594*, 2023.
- [ENO<sup>+</sup>21] Nelson Elhage, Neel Nanda, Catherine Olsson, Tom Henighan, Nicholas Joseph, Ben Mann, Amanda Askell, Yuntao Bai, Anna Chen, Tom Conerly, Nova DasSarma, Dawn Drain, Deep Ganguli, Zac Hatfield-Dodds, Danny Hernandez, Andy Jones, Jackson Kernion, Liane Lovitt, Kamal Ndousse, Dario Amodei, Tom Brown, Jack Clark, Jared Kaplan, Sam McCandlish, and Chris Olah. A mathematical framework for transformer circuits. *Transformer Circuits Thread*, 1(1):12, 2021. <https://transformer-circuits.pub/2021/framework/index.html>.
- [Gor04] Jan Gorodkin. Comparing two k-category assignments by a k-category correlation coefficient. *Computational biology and chemistry*, 28(5-6):367–374, 2004.
- [HLO22a] Yang-Hui He, Kyu-Hwan Lee, and Thomas Oliver. Machine-learning number fields. *Math. Comput. Geom. Data*, 2(1):49–66, 2022.
- [HLO22b] Yang-Hui He, Kyu-Hwan Lee, and Thomas Oliver. Machine-learning the Sato-Tate conjecture. *J. Symbolic Comput.*, 111:61–72, 2022.
- [HLO23] Yang-Hui He, Kyu-Hwan Lee, and Thomas Oliver. Machine learning invariants of arithmetic curves. *J. Symbolic Comput.*, 115:478–491, 2023.
- [HLOP24] Yang-Hui He, Kyu-Hwan Lee, Thomas Oliver, and Alexey Pozdnyakov. Murmurations of elliptic curves. *Experimental Mathematics*, pages 1–13, 2024.
- [HLV24] Michael Hanna, Ollie Liu, and Alexandre Variengien. How does gpt-2 compute greater-than?: Interpreting mathematical abilities in a pre-trained language model. *Advances in Neural Information Processing Systems*, 36, 2024.
- [KV23] Matija Kazalicki and Domagoj Vlah. Ranks of elliptic curves and deep neural networks. *Res. Number Theory*, 9(3):Paper No. 53, 21, 2023.
- [LKN<sup>+</sup>22] Ziming Liu, Ouail Kitouni, Niklas S Nolte, Eric Michaud, Max Tegmark, and Mike Williams. Towards understanding grokking: An effective theory of representation learning. *Advances in Neural Information Processing Systems*, 35:34651–34663, 2022.
- [LMF24] The LMFDB Collaboration. The L-functions and modular forms database. <https://www.lmfdb.org>, 2024. [Online; accessed 29 December 2024].
- [Mat75] Brian W Matthews. Comparison of the predicted and observed secondary structure of t4 phage lysozyme. *Biochimica et Biophysica Acta (BBA)-Protein Structure*, 405(2):442–451, 1975.
- [NCL<sup>+</sup>23] Neel Nanda, Lawrence Chan, Tom Lieberum, Jess Smith, and Jacob Steinhardt. Progress measures for grokking via mechanistic interpretability. *arXiv preprint arXiv:2301.05217*, 2023.
- [Poz24] Alexey Pozdnyakov. Predicting root numbers with neural networks. *arXiv*, 2024. arXiv:math.NT:2403.14631v1.
- [QB23] Philip Quirke and Fazl Barez. Understanding addition in transformers. *arXiv preprint arXiv:2310.13121*, 2023.
- [SAWL24] Eshika Saxena, Alberto Alfarano, Emily Wenger, and Kristin Lauter. Teaching transformers modular arithmetic at scale. *arXiv preprint arXiv:2410.03569*, 2024.
- [Ser81] Jean-Pierre Serre. Quelques applications du théoreme de densité de chebotarev. *Publications Mathématiques de l’IHÉS*, 54:123–201, 1981.
- [Sut] Andrew V. Sutherland. A set of isogeny classes of elliptic curves of conductor up to  $10^7$ . <https://math.mit.edu/~edgarc/data/ECQ7.txt>.

- [SW02] William A. Stein and Mark Watkins. A database of elliptic curves—first report. In *Algorithmic number theory (Sydney, 2002)*, volume 2369 of *Lecture Notes in Comput. Sci.*, pages 267–275. Springer, Berlin, 2002.
- [VSP<sup>+</sup>17] Ashish Vaswani, Noam Shazeer, Niki Parmar, Jakob Uszkoreit, Llion Jones, Aidan N Gomez, Łukasz Kaiser, and Illia Polosukhin. Attention is all you need. In *Advances in Neural Information Processing Systems*, volume 30, pages 5998–6008. Curran Associates, Inc., 2017.
- [ZLTA24] Ziqian Zhong, Ziming Liu, Max Tegmark, and Jacob Andreas. The clock and the pizza: Two stories in mechanistic explanation of neural networks. *Advances in Neural Information Processing Systems*, 36, 2024.

DEPARTMENT OF MATHEMATICS, HOWARD UNIVERSITY, 204 ACADEMIC SERVICE BUILDING B WASHINGTON, D.C. 20059 USA

*Email address:* [angelica.babei@howard.edu](mailto:angelica.babei@howard.edu)

*URL:* <https://angelicababei.com>

FAIR, META – CERMICS, ECOLE DES PONTS

*Email address:* [fcharton@meta.com](mailto:fcharton@meta.com)

DEPARTMENT OF MATHEMATICS, MASSACHUSETTS INSTITUTE OF TECHNOLOGY, 77 MASSACHUSETTS AVE., CAMBRIDGE, MA 02139, USA

*Email address:* [edgarc@mit.edu](mailto:edgarc@mit.edu)

*URL:* <https://edgarcosta.org>

DEPARTMENT OF MATHEMATICS, TEMPLE UNIVERSITY, PHILADELPHIA, PA, 19122, USA.

*Email address:* [xiaoyu.huang@temple.edu](mailto:xiaoyu.huang@temple.edu)

DEPARTMENT OF MATHEMATICS, UNIVERSITY OF CONNECTICUT, STORRS, CT 06269, USA

KOREA INSTITUTE FOR ADVANCED STUDY, SEOUL 02455, REPUBLIC OF KOREA

*Email address:* [khlee@math.uconn.edu](mailto:khlee@math.uconn.edu)

*URL:* <https://khlee-math.github.io/>

ICERM, 121 S MAIN ST, PROVIDENCE, RI 02903

*Email address:* [david@lowryduda.com](mailto:david@lowryduda.com)

*URL:* <https://davidlowryduda.com>

SYDNEY MATHEMATICAL RESEARCH INSTITUTE, UNIVERSITY OF SYDNEY, CITY ROAD, CAMPERDOWN, SYDNEY, NSW 2006, AUSTRALIA

*Email address:* [ashvni.narayanan@sydney.edu.au](mailto:ashvni.narayanan@sydney.edu.au)

DEPARTMENT OF MATHEMATICS, PRINCETON UNIVERSITY, PRINCETON, NJ, 08544-1000, USA.

*Email address:* [ap5763@princeton.edu](mailto:ap5763@princeton.edu)